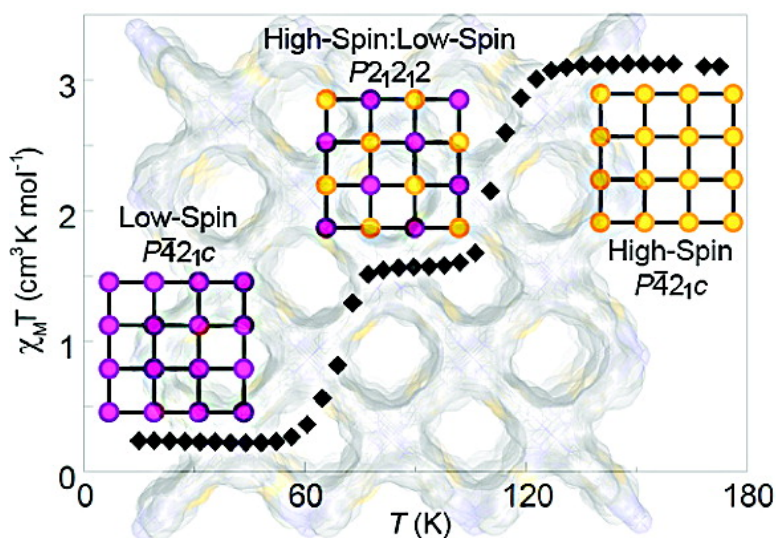## Article

Elucidating the Mechanism of a Two-Step Spin Transition in a Nanoporous Metal#Organic Framework

Gregory J. Halder, Karena W. Chapman, Suzanne M. Neville, Boujemaa Moubaraki, Keith S. Murray, Jean-Franc#ois Le#tard, and Cameron J. Kepert

More About This Article

Additional resources and features associated with this article are available within the HTML version:

- Supporting Information
- Access to high resolution figures
- Links to articles and content related to this article
- Copyright permission to reproduce figures and/or text from this article

View the Full Text HTML

Elucidating the Mechanism of a Two-Step Spin Transition in a Nanoporous Metal−Organic Framework

Gregory J. Halder,[†,‡] Karena W. Chapman,[§] Suzanne M. Neville,[||]
Boujemaa Moubaraki,[||] Keith S. Murray,[||] Jean-François Létard,[⊥] and
Cameron J. Kepert*,[†]

School of Chemistry, The University of Sydney, NSW 2006, Australia, Materials Science Division, Argonne National Laboratory, Argonne, Illinois 60439, X-ray Science Division, Advanced Photon Source, Argonne National Laboratory, Argonne, Illinois 60439, School of Chemistry, Monash University, VIC 3800, Australia, and Laboratoire des Sciences Moléculaires, ICMCB (CNRS UPR 9048), Université Bordeaux I, 33608 Pessac, France

Received August 28, 2008; E-mail: c.kepert@chem.usyd.edu.au

Abstract: The nanoporous metal−organic framework, $Fe(bpe)_2(NCS)_2 \cdot 3(acetone)$, **SCOF-4(Ac)** (where bpe is 1,2-bis(4′-pyridyl)ethane), displays a two-step spin crossover (SCO) transition (65−155 K) that is sensitive to the presence of acetone guest molecules. Structural analyses have revealed a structural phase transition, from tetragonal ($P\bar{4}2_1c$) to orthorhombic ($P2_12_12$), associated with the spin transition that defines a checkerboard-like ordering of spin sites at the high-spin:low-spin plateau. The reversible desorption of the acetone guest species is accompanied by a complex series of structural phase transitions that describe a dramatic flexing of the structure. The thermal trapping of a metastable state with ~20−25% high-spin character was observed both magnetically and structurally upon rapid quenching of **SCOF-4(Ac)** to 10 and 25 K, respectively. The light-induced excited spin state trapping (LIESST) effects for **SCOF-4(Ac)** show a 55% excitation of a metastable HS state at 10 K and a characteristic T(LIESST) value of 52 K.

Introduction

Spin crossover (SCO) is a fundamental phenomenon in molecular magnetism that involves the reversible switching of a metal center between high-spin (HS) and low-spin (LS) electronic states as a function of some external perturbation, such as temperature, pressure, or light-irradiation.[1] Much of the interest in SCO research has focused on the bistability of highly cooperative systems that can exist in two different electronic states under the same conditions depending on the history of the system, with potential applications in memory devices and electronic displays.[2,3] Central to this research has been the goal of developing an understanding of the underlying mechanisms that drive cooperativity (i.e., the extent to which spin-state changes are propagated in the solid-state). In particular, systems exhibiting two-step spin conversions, where SCO proceeds *via* a HS:LS stabilized phase at the intermediate plateau (IP), offer a novel means for examining cooperativity. Parallel investigations of the magnetic and structural properties of these systems, including light-induced and thermally induced excited spin state

trapping effects (LIESST[2,4] and TIESST[5]), allow for a detailed investigation of the relative importance of cooperative versus anticooperative interactions between the switching metal centers.

In recent years, SCO research has intersected with the expansive field of coordination frameworks (or metal−organic frameworks; MOFs)[6,7] to generate a new class of SCO material where the switching centers are directly bridged by organic linker ligands into multidimensional networks.[8−12] Like coordination frameworks, spin crossover frameworks (SCOFs) have the potential to exhibit porosity and as such offer a unique platform to investigate the influence of absorbed guests on SCO

(1) (a) Gütlich, P.; Goodwin, H. A. *Top. Curr. Chem.* **2004**, *233*, 1–47. (b) Kahn, O. *Molecular Magnetism*; VCH: New York, 1993.
(2) Létard, J.-F.; Guionneau, P.; Goux-Capes, L. *Top. Curr. Chem.* **2004**, *235*, 221–249.
(3) Kahn, O.; Martinez, C. J. *Science* **1998**, *279*, 44–48.
(4) Gütlich, P.; Hauser, A.; Spiering, H. *Angew. Chem., Int. Ed.* **1994**, *33*, 2024–2054.
(5) Le Bris, R.; Mathonière, C.; Létard, J.-F. *Chem. Phys. Lett.* **2006**, *426*, 380–386.
(6) Kepert, C. J. *Chem. Commun.* **2006**, 695–700.
(7) (a) Kitagawa, S.; Kitaura, R.; Noro, S. *Angew. Chem., Int. Ed.* **2004**, *43*, 2334–2375. (b) James, S. L. *Chem. Soc. Rev.* **2003**, *32*, 276–288. (c) Eddaoudi, M.; Moler, D. B.; Li, H. L.; Chen, B. L.; Reineke, T. M.; O'Keeffe, M.; Yaghi, O. M. *Acc. Chem. Res.* **2001**, *34*, 319–330. (d) Hoskins, B. F.; Robson, R. *J. Am. Chem. Soc.* **1990**, *112*, 1546–1554.
(8) Neville, S. M.; Halder, G. J.; Chapman, K. W.; Duriska, M. B.; Southon, P. D.; Cashion, J. D.; Létard, J.-F.; Moubaraki, B.; Murray, K. S.; Kepert, C. J. *J. Am. Chem. Soc.* **2008**, *130*, 2869–2876.
(9) Neville, S. M.; Moubaraki, B.; Murray, K. S.; Kepert, C. J. *Angew. Chem., Int. Ed.* **2007**, *46*, 2059–2062.
(10) (a) Murray, K. S.; Kepert, C. J. *Top. Curr. Chem.* **2004**, *233*, 195–228. (b) Niel, V.; Thompson, A. L.; Muñoz, M. C.; Galet, A.; Goeta, A. E.; Real, J. A. *Angew. Chem., Int. Ed.* **2003**, *42*, 3760–3763. (c) Niel, V.; Martinez-Agudo, J. M.; Muñoz, M. C.; Gaspar, A. B.; Real, J. A. *Inorg. Chem.* **2001**, *40*, 3838–3839.
(11) Halder, G. J.; Kepert, C. J.; Moubaraki, B.; Murray, K. S.; Cashion, J. D. *Science* **2002**, *298*, 1762–1765.
(12) Real, J. A.; Andres, E.; Muñoz, M. C.; Julve, M.; Granier, T.; Bousseksou, A.; Varret, F. *Science* **1995**, *268*, 265–267.
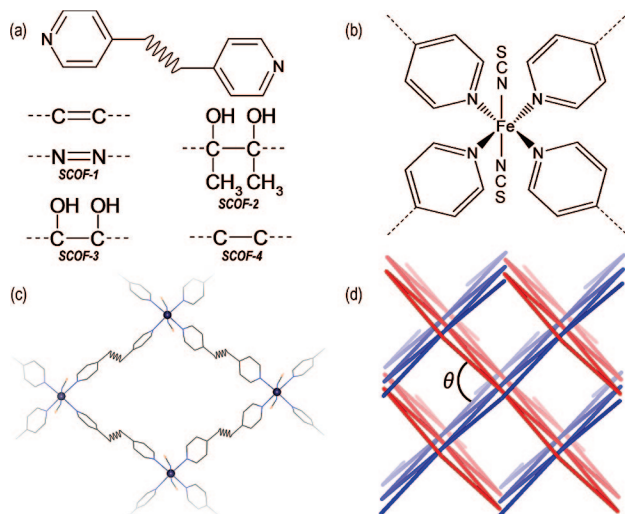
Figure 1. (a) Schematic representation of ligand variation within the SCOF series. (b) The Fe(II)(pyridyl)$_4$(*trans*-thiocyanate)$_2$ coordination environment. (c) Representation of the connectivity in a (4,4) Fe(bpe)$_2$ rhombic-grid. (d) A diagrammatic representation of the 2-fold interpenetration of extended Fe(bpe)$_2$ rhombic-grids as viewed along the crystallographic *c*-axis (where θ is the angle of interpenetration).

behavior. Indeed, the interplay between the host−guest and SCO properties in porous SCOFs has afforded advanced materials with rich and complex structure−function relationships. While examples of porous SCOFs are still relatively few, a versatile family of materials has emerged based on the extension of the discrete Fe(II)(pyridyl)$_4$(*trans*-NCS)$_2$ chromophore using linearly bridging exobidentate pyridyl-based ligands (L).[8,9,11,12] These SCOFs, with the general formula Fe(NCS)$_2$(L)$_2$·*x*(guest), consist of doubly interpenetrating rhombic grids (2 × (4,4) nets), defining one-dimensional pores that account for up to 39% of their total volume (Figure 1). Despite their structural similarities, these materials have shown a diverse range of guest-dependent structural and SCO features due in part to a structural flexibility associated with the interpenetration and associated variance in the host−host and host−guest interactions.

The accurate elucidation of the often complex structure−function relationships in functional porous materials, such as SCOFs and other advanced MOFs, presents a crucial step in their advancement.[6] For example, their open network structures are particularly susceptible to structural phase transformations, either as a function of temperature and/or guest desorption/resorption, that are likely to have dramatic effects on their functional properties. This requires the development of *in situ* structural techniques, such as X-ray and neutron diffraction, to precisely monitor the structural response of materials under the conditions in which they perform their desired functions.[8,13−15] While the implementation of *in situ* techniques can be challenging, they promise an unparalleled insight into not only major structural changes, such as phase transformations, but also many other more subtle structural variants, such as those associated with framework dynamics and the rearrangement of host−guest interactions.[13]

Here, we present the structural and magnetic characterization of the new SCOF material Fe(bpe)$_2$(NCS)$_2$·3(acetone) (**SCOF-4(Ac)**), which exhibits a two-step SCO that is sensitive to the presence of the acetone guest molecules. Complementary single crystal and *in situ* synchrotron-based powder X-ray diffraction techniques have revealed a series of intricate structural phase transitions associated with not only the SCO properties but also desorption and resorption of the acetone guest species.

Experimental Section

Synthesis. Yellow crystals of **SCOF-4(Ac)** were prepared by slow diffusion of bpe (60 mg, 0.33 mmol) with a mixture of iron(II) perchlorate (42 mg, 0.17 mmol) and ammonium thiocyanate (25 mg, 0.33 mmol) in acetone.

Magnetic Susceptibility Measurements. Initial magnetic susceptibility measurements were made using a Quantum Design MPMS 5 SQUID instrument operating under a field of 1 T. The sample was found to be highly sensitive to solvent loss, and reliable data were only obtained by sealing the sample in a quartz tube with a small amount of acetone. The sample also exhibited unusually slow relaxation kinetics and required long equilibration times to achieve agreeable heating and cooling data. These data and additional measurement details are included in the Supporting Information. For the desorbed analogue **SCOF-4**, a sample of **SCOF-4(Ac)** was heated at 90 °C under vacuum for 2 h. This sample was then immersed in a few drops of acetone to yield the resorbed sample, **r-SCOF-4(Ac)**.

Photomagnetic characterization was carried out using a Kr$^+$ laser coupled through an optical fiber into the cavity of the SQUID magnetometer. *Light-induced excited spin state trapping* (LIESST) experiments by magnetic susceptibility were carried out using a MPMS-55 Quantum Design SQUID magnetometer operating at 2 T in the 10−260 K range. A small amount of polycrystalline sample was suspended in grease to inhibit desorption. The suspended sample (∼0.1 mg) was then prepared in a thin layer to promote full penetration of the irradiated light. The sample mass was obtained by comparing its thermal spin transition behavior with a larger, accurately weighed sample.[16] Promptly after preparation, the sample was loaded in the magnetometer and cooled rapidly (∼10 K min^{-1}) to 200 K as a further preventative measure against desorption. Magnetic susceptibility data were first collected for the thermal spin transition on cooling to 10 K. The sample, now in the LS state, was then irradiated with green light ($\lambda = 530$ nm) until photosaturation was achieved (∼2.5 h). After terminating the irradiation, the temperature was increased at 1 K steps to 100 K. The *thermally induced excited spin state trapping* (TIESST) was investigated by quench-cooling from 200 to 10 K, trapping the material in a partially HS state. Magnetic susceptibility data were then collected at 1 K intervals with heating to 100 K. The extreme of the $\partial\chi_M T/\partial T$ versus T plot for the respective measurements gave the T(LIESST) and T(TIESST) values, defined as the temperature at which the trapped state information is erased.[5,16] Additionally, the time-dependence of the relaxation of the photoexcited state in the absence of irradiation was investigated at 40, 45, 48, 50, and 52 K (Supporting Information).

Single Crystal X-ray Diffraction (SC-XRD). Diffraction data for **SCOF-4(Ac)** at 150(2), 100(2), and 25(2) K (with either quench or slow cooling) were collected on separate crystals on a Bruker Smart 1000 CCD equipped with Mo Kα ($\lambda = 0.71073$ Å) radiation and Oxford Cryosystems nitrogen gas (100−200 K) and helium gas (25 K structures) open flow cryostats. Empirical absorption corrections within SADABS[17] were applied to the data sets reduced

(13) Halder, G. J.; Kepert, C. J. *J. Am. Chem. Soc.* **2005**, *127*, 7891−7900.
(14) (a) Chapman, K. W.; Halder, G. J.; Chupas, P. J. *J. Am. Chem. Soc.* **2008**, *130*, 10524−10526. (b) Chapman, K. W.; Chupas, P. J.; Maxey, E. R.; Richardson, J. W. *Chem. Commun.* **2006**, 4013−4015. (c) Chapman, K. W.; Chupas, P. J.; Kepert, C. J. *J. Am. Chem. Soc.* **2005**, *127*, 11232−11233.
(15) Millange, F.; Serre, C.; Guillou, N.; Férey, G.; Walton, R. I. *Angew. Chem., Int. Ed.* **2008**, *47*, 4100−4105.

(16) (a) Létard, J.-F. *J. Mater. Chem.* **2006**, *16*, 2550−2559. (b) Létard, J.-F.; Guionneau, P.; Nguyen, O.; Costa, J. S.; Marcén, S.; Chastanet, G.; Marchivie, M.; Goux-Capes, L. *Chem.−Eur. J.* **2005**, *11*, 4582−4589.
(17) Sheldrick, G. M. *SADABS. Empirical adsorption correction program for area detector data*; University of Göttingen, Germany, 1996.

with SAINT+.[18] The structures were solved with SHELXS-97[19] and refined with SHELXL-97.[20] Solvent accessible volumes were calculated within PLATON[21] using the VOID routine. CCDC reference numbers: 705393−705396. Single crystal variable temperature unit cell determinations were carried out during slow cooling from 200 to 25 K and on heating from 25 to 100 K (after quench cooling). The temperature was ramped at 20 K h^{-1} while diffraction images (3 sets of 20 images; 0.3° steps; 15−20 s exposure; and ~10 s readout time per image) were collected continuously within the SMART[18] interface.

Synchrotron-Based Powder X-ray Diffraction (S-PXRD). Polycrystalline samples of **SCOF-4(Ac)** were ground as a slurry in a small amount of anhydrous acetone, loaded into polyimide capillaries (0.9 mm diameter), immediately assembled into a flow cell apparatus,[22] and placed under a helium gas atmosphere at 260 K. Surface wetness was maintained throughout the loading process to prevent sample desorption. Supernatant acetone was removed by flowing helium gas through the sample at 260 K while monitoring the associated diffuse scattering in the diffraction data. The samples were maintained under either neat helium or acetone vapor-saturated helium gas flow for the duration of the experiment. The X-rays (20.15 keV, 0.61516 Å) available at the 1-BM beamline at the Advanced Photon Source at Argonne National Laboratory were used in combination with a MAR-345 imaging plate detector to record diffraction patterns. The sample temperature was controlled using an Oxford Cryosystems Cryostream 700 plus, and data were collected in 5 s exposures upon continuous ramping over the range 80 to 350 K, at 120 K h^{-1}. This corresponds to the collection of diffraction images at 4 K intervals. The raw images were processed using Fit-2D.[23] The sample-to-detector distance (599.828 mm) and tilt of the image plate relative to the beam were refined using a LaB$_6$ standard. Le Bail analyses of the diffraction data were performed within GSAS.[24] Details of the refinements are included in the Supporting Information.

Thermogravimetry. Measurements were carried out on a TA Instruments Hi-Res TGA 2950 Thermogravimetric Analyzer. To identify the approximate temperature of guest loss and thermal decomposition, the temperature was ramped at 2 °C min^{-1} from 20 to 500 °C. The resorption of acetone was investigated by the *ex situ* immersion of a sample of **SCOF-4** (desorbed by heating to 80 °C for 1 h) in acetone for 24 h before analyzing as described above.

Results

Magnetism. Variable temperature magnetic susceptibility measurements were used to probe the spin states and spin changes of **SCOF-4(Ac)**, revealing a two-step spin transition (Figure 2). At temperatures above 155 K, the $\chi_M T$ value remains approximately constant at 3.1−3.2 cm^3 mol^{-1}, indicative of HS, $S = 2$, iron(II) sites only. On further cooling, the $\chi_M T$ values decrease in two well defined steps, to minimum values below 65 K of approximately 0.3−0.4 cm^3 mol^{-1}, consistent with
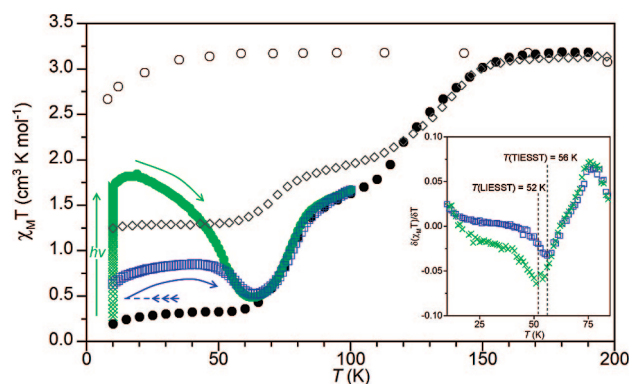

Figure 2. Temperature dependence of $\chi_M T$ in the range 10−200 K for **SCOF-4(Ac)** (●, thermal SCO; □ (blue), thermal trapping; × (green), irradiation at 530 nm followed by relaxation), **SCOF-4** (○), and a resorbed sample of **SCOF-4(Ac)** (◇). Inset: Plot of $\delta\chi_M T/\delta T$ versus temperature indicating T(LIESST) and T(TIESST) values of 52(2) and 56(2) K, respectively.

predominantly LS, $S = 0$, iron(II) sites. There is a further slight downturn in the $\chi_M T$ values below 15 K associated with zero field splitting effects of a minor residual HS fraction (less than 10%). The $T_{1/2}$ values (the temperature of 50% spin state conversion) for the two steps are 133 K for $T_{1/2}(1)$ and 80 K for $T_{1/2}(2)$. In the region 110−90 K, the rate of change in the $\chi_M T$ values shows a clear decrease centered around 1.6 cm^3 mol^{-1}, suggesting a near 1:1 ratio of HS and LS iron(II) sites at the IP.

The TIESST of a partial HS state was achieved by rapidly cooling the sample to 10 K. The extent of trapping was dependent on the rate of cooling, with faster cooling rates resulting in larger fractions of HS sites. The thermal-trapping data shown in Figure 2 were achieved with a cooling rate of 100 K h^{-1} (the maximum cooling rate of the instrument) using the same sample loading as that for the photomagnetism measurements. Here, a $\chi_M T$ value of 0.63 cm^3 mol^{-1} at 10 K suggests *ca.* 20% HS trapping. Upon heating, the $\chi_M T$ values show a small increase to a maximum of 0.85 cm^3 mol^{-1} at 40 K, beyond which the thermally trapped state begins to relax with a T(TIESST) of 56(2) K (Figure 2, inset).

The photomagnetic properties of **SCOF-4(Ac)** were investigated by irradiating the $^1A_1 \rightarrow {^1T}$ absorption band with green light ($\lambda = 530$ nm) at 10 K (Figure 2). The $\chi_M T$ values at 10 K attained a maximum value of 1.71 cm^3 K mol^{-1}, indicating a *ca.* 55% photoexcitation of the HS state. We note that a higher percentage of trapped HS metastable species may be possible here with the use of a stronger laser. Without irradiation, the magnetic response between 10 and 20 K appears to be temperature independent, as there was an observed increase in $\chi_M T$ over this range, to a maximum of 1.84 cm^3 K mol^{-1}; this increase in $\chi_M T$ reflects that seen over the same temperature range in the thermal SCO and is attributed to zero-field splitting of the HS iron(II) sites. Over the range 20−70 K, without irradiation, the $\chi_M T$ values progressively relaxed to a minimum of 0.49 cm^3 K mol^{-1} at 62 K, coincident with the onset of the thermal SCO. This value is slightly higher than that observed at the same temperature for the thermal SCO (*ca.* 0.40 cm^3 K mol^{-1}), suggesting a competition between photoinduced excitation and relaxation times. The $\partial\chi_M T/\partial T$ versus T plot shows a characteristic T(LIESST) value of 52(2) K for **SCOF-4(Ac)** (Figure 2, inset). The relaxation kinetics of the metastable HS

(18) *SMART, SAINT and XPREP. Area Detector control and data integration and reduction software*; Bruker Analytical X-ray Instruments Inc.: Madison, WI, 1995.
(19) Sheldrick, G. M. *SHELXS-97. Program for crystal structure solution*; University of Göttingen: Germany, 1997.
(20) Sheldrick, G. M. *SHELXL-97. Program for crystal structure refinement*; University of Göttingen: Germany, 1997.
(21) Spek, A. L. *Acta Crystallogr.* **1990**, *A46*, 194–201.
(22) (a) Chupas, P. J.; Chapman, K. W.; Kurtz, C.; Hanson, J. C.; Lee, P. L.; Grey, C. P. *J. Appl. Crystallogr.* **2008**, *41*, 822–824. (b) Chupas, P. J.; Ciraolo, M. F.; Hanson, J. C.; Grey, C. P. *J. Am. Chem. Soc.* **2001**, *123*, 1694–1702.
(23) (a) Hammersley, A. P. ESRF Internal Report. , 1997; ESRF97HA02T. (b) Hammersley, A. P.; Svensson, S. O.; Hanfland, M.; Fitch, A. N.; Hausermann, D. *High Pressure Res.* **1996**, *14*, 235–248.
(24) Larson, A. C.; Dreele, R. B. V. *General Structure Analysis System (GSAS)*; Los Alamos National Laboratory Report LAUR 86-748; 2000.

Table 1. Crystal Data and Refinement Details for **SCOF-4(Ac)**

	SCOF-4(Ac)[150]	SCOF-4(Ac)[100]	SCOF-4(Ac)[25T]	SCOF-4(Ac)[25]
spin state	HS	HS:LS	LS:partial HS	LS
T/K	150	100	25	25
formula		$Fe(C_{12}H_{12}N_2)_2(NCS)_2 \cdot (C_3H_6O)_3$		
FW/gmo1^{-1}		714.72		
crystal system	orthorhombic	orthorhombic	orthorhombic	tetragonal
space group	$P2_12_12$	$P2_12_12$	$P2_12_12$	$P\bar{4}2_1c$
a/Å	15.114(3)	14.8646(18)	14.8257(16)	14.739(4)
b/Å	15.101(3)	14.9069(18)	14.8278(16)	
c/Å	16.842(3)	16.747(2)	16.7187(18)	16.662(9)
V/Å^3	3844.0(14)	3710.8(8)	3675.3(7)	3619(2)
ρ_{calc}/Mg m^{-3}	1.235	1.279	1.292	1.312
μ/mm^{-1}	0.541	0.560	0.566	0.574
data/restraints/parameters	8918/132/230	8720/126/239	7963/140/239	4117/18/195
$R(F)$ {$I > 2\sigma(I)$, all}/%	0.0865, 0.0985	0.0777/0.1027	0.0734, 0.0755	0.0809, 0.1192
$R_w(F^2)$ {$I > 2\sigma(I)$, all}/%	0.1712, 0.1782	0.1700/0.1843	0.1622, 0.1641	0.2043, 0.2378
GoF	1.175	1.180	1.180	1.107

Table 2. Selected Bond Lengths and Other Structural Parameters for **SCOF-4(Ac)**

	SCOF-4(Ac)[150]		SCOF-4(Ac)[100]		SCOF-4(Ac)[25T]		SCOF-4(Ac)[25]
	Fe(1)^{HS}	**Fe(2)^{HS}**	**Fe(1)^{HS}**	**Fe(2)^{LS}**	**Fe(1)$^{\sim HS}$**	**Fe(2)^{LS}**	
$\langle d_{Fe-N(py)} \rangle$/Å	2.205(6)	2.206(7)	2.192(7)	2.014(7)	2.122(7)	2.051(7)	2.053(7)
$\langle d_{Fe-N(CS)} \rangle$/Å	2.114(7)	2.092(6)	2.053(7)	1.970(7)	2.046(7)	1.957(7)	1.964(5)
Σ/deg	39.5	21.0	15.6	19.1	26.3	16.0	13.6
Py-Fe-Py torsion/deg	74.6(8)	68.1(8)	72.1(8)	76.2(9)	72.7(8)	75.4(8)	73.5(6)
C(Ac)$\cdots$O(Ac)/Å	2.95–3.39		2.83–3.37		2.67–3.15		3.05–3.27
S$\cdots\pi$/Å	4.08–4.34	4.17–4.25	3.98–4.18	4.18–4.23	4.00–4.16	4.09–4.16	4.04–4.10
grid diagonals/Å^2	16.84 × 21.36		16.75 × 21.05		16.72 × 20.97		16.62 × 20.84
pore diameter/Å	5.06		4.96		4.92		4.81
pore volume/%	39.2		38.5		38.3		38.5

fraction in the absence of irradiation exhibited stretched exponential decay consistent with low cooperativity in this system.

The $\chi_M T$ values for the fully desorbed material **SCOF-4** are essentially constant at 3.18 cm^3 mol^{-1}, as is consistent with the presence of only HS iron(II) centers, with zero field splitting effects resulting in a minor decrease below 25 K (Figure 2). This desorbed material was then immersed in liquid acetone to give a resorbed sample ***r*-SCOF-4(Ac)**. Subsequent magnetic measurements again revealed a two-step spin transition, but the completeness of the transition to LS was significantly diminished. The first step is associated with a ~40% conversion of HS to LS ($T_{1/2}(1) = 133$ K), while the second smaller step accounts for only ~20% HS to LS conversion ($T_{1/2}(2) = 76$ K). The diminished SCO for the resorbed sample may reflect incomplete resorption, a significant loss of sample integrity during the desorption−resorption process, or possibly a different alignment of the guests within the channels.

Single Crystal X-ray Diffraction. Single crystal refinement parameters for the HS (**SCOF-4(Ac)[150]**), HS:LS (**SCOF-4(Ac)[100]**), thermally trapped (**SCOF-4(Ac)[25T]**), and LS (**SCOF-4(Ac)[25]**) states of **SCOF-4(Ac)** are shown in Table 1 (Note: Due to different experimental protocols, the **SCOF-4(Ac)[25T]** (quench-cooled to 25 K) state is not directly comparable to the thermally trapped state from the magnetic measurements (cooled rapidly at 100 K h^{-1})). Relevant structural parameters, including average iron(II)−nitrogen bond lengths ($\langle d_{Fe-N} \rangle$) and the octahedral distortion parameter (Σ), are presented in Table 2. The $\langle d_{Fe-N} \rangle$ parameters can be used to quantify the iron(II) spin state (LS, ~2.0 Å; HS, ~2.2 Å). The Σ parameter (the sum of the deviations from 90° for the 12 *cis* angles of the iron(II) octahedra) is a useful tool in quantifying the changes in the iron(II) environment associated with SCO, where smaller values

(i.e., less distorted octahedra) typically indicate the stabilization of the LS state.[25]

Initial analysis of the data suggested tetragonal symmetry at all studied temperatures. Space group assignment was nontrivial, as almost all tetragonal space groups provided adequate solutions but most refined poorly. A detailed manual examination of the systematic absences indicated the high symmetry tetragonal space group $P\bar{4}2_1c$, which led to convincing refinements for all data sets. For the 100 K and quench-cooled 25 K data, this solution has a single iron(II) site with intermediate HS:LS iron(II)−nitrogen bond lengths (~2.10 and ~2.05 Å, respectively). Treatment of the final solutions with the ADDSYM routine within PLATON[21] detected additional symmetry/pseudosymmetry and suggested the higher symmetry space group $P4/ncc$. This space group has been observed for a number of closely related systems[9,12] but for the present system was not consistent with the systematic absences and yielded solutions with refinement indices approximately double those for $P\bar{4}2_1c$. Subsequent S-PXRD studies (see below) unambiguously confirmed that the correct symmetry between 80 and 170 K was the orthorhombic space group $P2_12_12$ (a direct subgroup of $P\bar{4}2_1c$). For all but **SCOF-4(Ac)[25]**, refinement in $P2_12_12$ gave an improved fit and revealed the long-range structural ordering of the HS and LS iron(II) sites for **SCOF-4(Ac)[100]** and **SCOF-4(Ac)[25T]**, which is discussed in more detail below. Refinement of **SCOF-4(Ac)[25]** in $P2_12_12$ gave a highly unstable and inferior result due predominantly to severe correlation between refinement variables for the doubled asymmetric unit. Further details pertaining to space group assignment are included in the Supporting Information.

(25) Guionneau, P.; Marchivie, M.; Bravic, G.; Létard, J.-F.; Chasseau, D. *Top. Curr. Chem.* **2004**, *234*, 97−128.

Table 3. Distances and Angles for Interframework Interactions[a]

	Fe···Fe (Å)	edge···π (Å)	S···π (Å)	C···π/S (Å)	H···π/S (Å)	>C–H···π/S (deg)
SCOF-4(Ac)[150]						
C16–H16(Fe2)···N1>C5(Fe1)	8.48	3.83		3.75	3.11	126
C9–H9(Fe2)···N4>C22(Fe1)	8.36	3.90		3.92	3.35	121
C2–H2(Fe1)···N3>C17(Fe2)	8.48	3.97		3.95	3.33	125
C19–H19(Fe1)···N2>C10(Fe2)	8.36	3.98		3.94	3.21	136
S25(Fe1)···N1>C5(Fe1)	10.68		4.08	3.42	3.24	93
S25(Fe1)···N4>C22(Fe1)	10.68		4.34	3.80	3.61	94
S26(Fe2)···N2>C10(Fe2)	10.68		4.17	3.69	3.66	85
S26(Fe2)···N3>C17(Fe2)	10.68		4.25	3.64	3.50	91
SCOF-4(Ac)[100]						
C16–H16(Fe2)···N1>C5(Fe1)	8.39	3.70		3.80	2.96	136
C9–H9(Fe2)···N4>C22(Fe1)	8.56	3.86		3.81	3.10	133
C2–H2(Fe1)···N3>C17(Fe2)	8.39	3.93		3.88	3.31	121
C19–H19(Fe1)···N2>C10(Fe2)	8.56	3.93		3.91	3.25	128
S25(Fe1)···N1>C5(Fe1)	10.53		3.98	3.40	3.30	88
S25(Fe1) ···N4>C22(Fe1)	10.53		4.18	3.80	3.61	89
S26(Fe2)···N2>C10(Fe2)	10.53		4.18	3.60	3.47	89
S26(Fe2)···N3>C17(Fe2)	10.53		4.23	3.50	3.26	97
SCOF-4(Ac)[25T]						
C16–H16(Fe2)···N1>C5(Fe1)	8.41	3.77		3.68	3.01	128
C9–H9(Fe2)···N4>C22(Fe1)	8.32	3.85		3.78	3.03	137
C2–H2(Fe1)···N3>C17(Fe2)	8.41	3.91		3.84	3.15	131
C19–H19(Fe1)···N2>C10(Fe2)	8.32	3.89		3.87	3.25	124
S25(Fe1)···N1>C5(Fe1)	10.48		4.00	3.36	3.17	93
S25(Fe1) ···N4>C22(Fe1)	10.48		4.16	3.63	3.46	92
S26(Fe2)···N2>C10(Fe2)	10.48		4.09	3.57	3.52	85
S26(Fe2)···N3>C17(Fe2)	10.48		4.16	3.47	3.28	94
SCOF-4(Ac)[25]						
C4–H4···N1>C5	8.37	3.88		3.82	3.13	131
C9–H9···N2>C10	8.29	3.82		3.74	3.05	131
S13···N1>C5	10.42		4.10	3.53	3.42	89
S13···N2>C10	10.42		4.04	3.41	3.28	90

[a] Estimated errors do not exceed 0.01 Å or 0.5°. π: calculated centroid of the pyridyl units (face). Edge: the average position of the two pyridyl carbon atoms representative of the interacting edge.

The general structural motif of doubly interpenetrating two-dimensional rhombic grids is maintained for all four structural determinations irrespective of the symmetry. For the orthorhombic phases, there are two distinct iron(II) environments (Fe1 and Fe2). At 150 K, the $\langle d_{Fe-N}\rangle$ values show that both environments are in the HS state; however, the Fe1 site shows an Σ parameter almost double that of Fe2. As expected, it is the more regular Fe2 site that switches at the higher temperature, with the $\langle d_{Fe-N}\rangle$ at the IP (**SCOF-4(Ac)[100]**) unambiguously showing the Fe1 and Fe2 sites in the HS and LS states, respectively. These sites occupy alternating positions within the rhombic grids, generating a checkerboard-like arrangement of spin sites. Interestingly, SCO at the Fe2 site is associated with a more regular coordination environment about the Fe1 site, as evidenced by the decrease in Σ from 39.5 to 15.6°. Upon slow-cooling to 25 K (**SCOF-4(Ac)[25]**), the material undergoes a structural phase transition to tetragonal symmetry that defines a single crystallographically distinct iron(II) center with a $\langle d_{Fe-N}\rangle$

value indicative of the LS state. However, if a crystal is quench-cooled to 25 K (**SCOF-4(Ac)[25T]**), a significant HS population can be trapped, as also observed for the magnetic susceptibility measurements. There is a marked difference in the $\langle d_{Fe-N}\rangle$ values for the two distinct iron(II) sites in this now orthorhombic phase; while the values for Fe2 are consistent with the LS state, those at the Fe1 site suggest an approximate 50% HS population.

The angle between the interpenetrated grids (θ), which for the tetragonal structure is constrained by symmetry to be 90°, exhibits a slight scissoring for the orthorhombic phases. This angle is related to the difference between the a and b lattice parameters ($\theta = 2\arctan(a/b)$); however, the pseudomerohedral twinning results in a relative inaccuracy in the parameters derived from SC-XRD compared to those from the S-PXRD data (Table 4). The interpenetration defines cylindrical one-dimensional pores along the crystallographic c-axis of approximately 5 Å in diameter. These channels account for 39% of the total volume and are filled with acetone guest molecules

Table 4. Lattice Parameters for the Various Phases Identified from *in Situ* S-PXRD Experiments

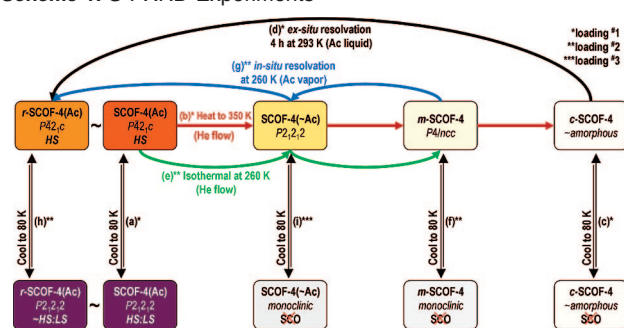| exp	phase	T (K)	space group	spin-state	a (Å)	b (Å)	c (Å)	V (Å³)	θ (deg)
(a)	**SCOF-4(Ac)**	260	$P\bar{4}2_1c$	HS	15.21898(12)		16.7665(2)	3883.42(6)	90
(a)	**SCOF-4(Ac)**	148	$P2_12_12$	HS	15.0923(4)	15.0385(3)	16.8252(3)	3818.72(14)	90.205(4)
(a)	**SCOF-4(Ac)**	80	$P2_12_12$	HS:LS	14.7549(3)	14.8406(3)	16.6546(3)	3646.89(11)	89.668(4)
(d)	**r-SCOF-4(Ac)**	260	$P\bar{4}2_1c$	HS	15.2499(4)		16.7629(7)	3898.4(2)	90
(e)	**SCOF-4(∼Ac)**	260	$P2_12_12$	HS	14.9366(3)	15.5476(3)	16.6908(3)	3876.07(13)	87.704(4)
(e)	**m-SCOF-4**	260	$P4/ncc$	HS	15.24479(11)		16.67550(18)	3875.45(6)	90
(h)	**r-SCOF-4(Ac)**	260	$P\bar{4}2_1c$	HS	15.25284(10)		16.75585(18)	3898.24(5)	90
(i)	**r-SCOF-4(Ac)**	191	$P2_12_12$	HS	15.1862(7)	15.1316(7)	16.8084(5)	3862.4(2)	89.794(8)
(i)	**r-SCOF-4(Ac)**	80	$P2_12_12$	HS:LS	14.9777(6)	14.8497(6)	16.6495(4)	3703.1(2)	89.508(7)
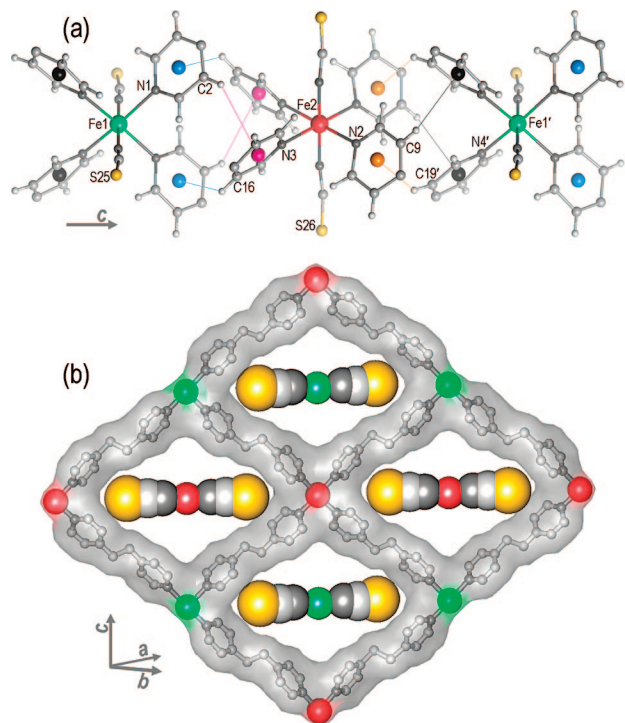
Figure 3. (a) 4-fold pyridyl embraces between alternating Fe1 (green) and Fe2 (red) sites along the *c*-axis for the orthorhombic phases (S, yellow; C/N, gray; H, white). Equivalent pyridyl groups are shown with matching centroid markers (N1 > C5, blue; N2 > C10, orange; N3 > C17, pink; N4 > C22, black). (b) Cross-sectional representation of the S···π contacts that propagate in the *ab* plane between equivalent Fe sites; hydrogen atoms have been omitted for clarity.

(26) Dance, I.; Scudder, M. *Chem.—Eur. J.* **1996**, *2*, 481–486.

Scheme 1. S-PXRD Experiments[a]

[a] (a) Cooling and Heating of **SCOF-4(Ac)** through the SCO Region; (b) Rigorous Desorption of **SCOF-4(Ac)** to the Collapsed Phase, *c*-**SCOF-4**, by Heating to 350 K; (c) Temperature Dependence of *c*-**SCOF-4**; (d) *ex Situ* Resorption of *c*-**SCOF-4** to *r*-**SCOF-4(Ac)** by Immersion in Acetone for 4 h; (e) Careful Desorption of **SCOF-4(Ac)** to the Metastable Tetragonal Phase, *m*-**SCOF-4**, at 260 K; (f) Temperature Dependence of *m*-**SCOF-4**; (g) *in Situ* Resorption of *m*-**SCOF-4** to *r*-**SCOF-4(Ac)** with Acetone Vapor; (h) Temperature Dependence of *r*-**SCOF-4(Ac)**; (i) Temperature Dependence of the Partially Desorbed Phase **SCOF-4(~Ac).**

in **SCOF-4(Ac)**. Interatomic distances between adjacent guests are consistent with hydrogen bonding interactions (C−H···O = 2.7−3.4 Å), but no interactions are apparent between the guest molecules and the framework. Consequently, the pore structure and guest location are essentially unaffected by the changes in symmetry and spin state.

Comparison of the structural changes during the phase transition between tetragonal and orthorhombic symmetry suggests that the three-dimensional ordering of inequivalent iron(II) sites in the orthorhombic phase is driven by an interplay between relatively subtle cooperative versus anticooperative van der Waals contacts and π···π interactions. The closest Fe···Fe separations between the interpenetrated grids form aryl embrace interactions[26] that consist of four cyclic edge-to-face π···π interactions (Figure 3a). In the orthorhombic phase, these interactions appear to be responsible for the stabilization of alternating, inequivalent iron(II) sites along the *c*-direction, as evidenced by the lengthening of half of these interactions with respect to the tetragonal **SCOF-4(Ac)**[25] structure (Table 3) and associated variation in the iron(II) coordination geometries of neighboring sites (Table 2). The steric constraints of this aryl embrace therefore likely contribute an anticooperative SCO effect, in which the synchronous SCO-induced expansion of neighboring iron(II) centers is disfavored with warming through the low temperature half-SCO step and leads instead to chains of alternating HS (Fe1) and LS (Fe2) sites. In contrast, close pyridyl-to-sulfur contacts (π···S)[27] that propagate as grids in the *ab* plane between equivalent iron(II) centers (i.e., ···S(CN)−Fe1−(NC)S···Py−Fe1−Py···S(CN)−Fe1−(NC)S···Py−Fe1;

Figure 3b) appear to promote cooperativity between Fe sites to generate layers that are fully HS or LS in the 50:50 HS:LS structure; the mechanism for this appears to be the retention of optimal π···S geometries following the relative translation of the thiocyanate and pyridyl units with SCO at the Fe1 site (Table 3).

Synchrotron-Based Powder X-ray Diffraction. A series of S-PXRD experiments were undertaken to investigate the structural changes associated with SCO and also with the desorption and resorption of the acetone guest molecules (Scheme 1). These predominantly *in situ* experiments involved the collection of either temperature- or time-dependent diffraction data with samples maintained under a controlled atmosphere using a custom-built flow cell and vapor saturator setup. The refined lattice parameters for experiments (a), (b), and (e) are shown in Figure 4, and additional selected data are included in Table 4. Detailed figures for each of the experiments, including peak evolutions, representative patterns and fits, and plots of refined lattice parameters, are included in the Supporting Information. The sections (a) to (i), below, correlate with the labels in Scheme 1.

(a) The variable temperature diffraction data for the as synthesized phase, **SCOF-4(Ac)**, collected with cooling from 260 to 80 K (Figure 4), showed a subtle symmetry lowering at 160 K, approximately 20 K higher in temperature than onset of a lattice contraction associated with the spin transition. Le Bail analyses of the high temperature data were consistent with a tetragonal space group of $P\bar{4}2_1c$ as observed for the LS (slow-cooled) SC-XRD structural refinements. The most diagnostic changes associated with the symmetry lowering phase transition were the appearance of two new peaks around 7° in 2θ, which were inconsistent with either $P\bar{4}2_1c$ or its tetragonal subgroup $P\bar{4}$. Investigation of the orthorhombic subgroups of $P\bar{4}2_1c$ identified the low symmetry phase as $P2_12_12$, as was observed for the 100 K SC-XRD structural refinement. The symmetry lowering defines a split of the tetragonal *a* parameter into unique orthorhombic *a* and *b* parameters, associated with a slight scissoring of the interpenetrating layers, and results in an increase in the number of unique iron(II) sites from one to two. This phase remains throughout the measured SCO region with further cooling to 80 K. Interestingly, the *a* parameter exhibits a more dramatic change through the SCO region than the *b*
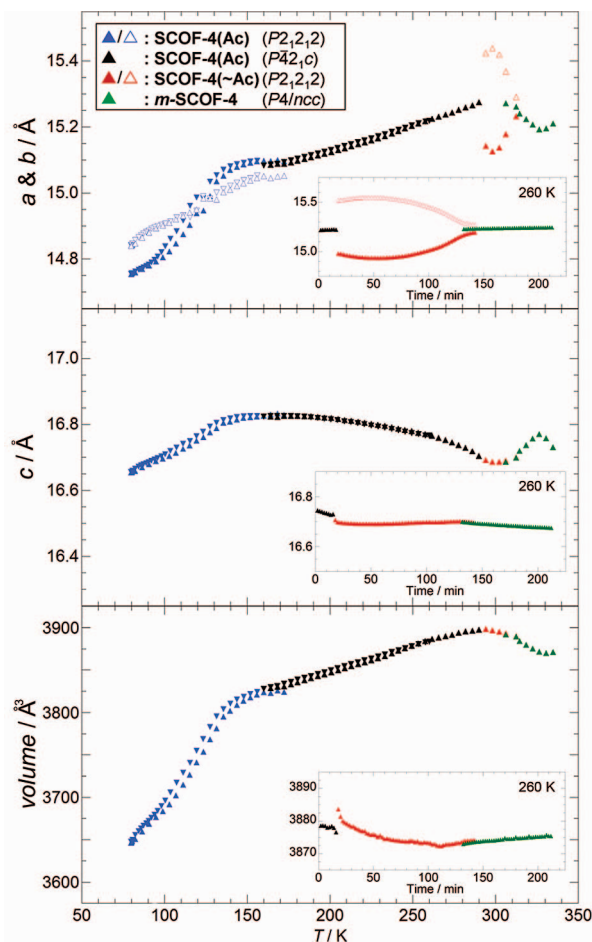
Figure 4. Temperature-dependent lattice parameters for **SCOF-4(Ac)** from Le Bail analysis of S-PXRD data collected on cooling from 260 to 80 K (▼) and subsequent heating to 340 K (▲). Insets show time-dependent lattice parameters during the desorption process while the sample was maintained at 260 K for 210 min. The *a* and *b* parameters of the orthorhombic phases are shown as filled and hollow symbols, respectively. Errors are within the size of the data points.

parameter, with respective contractions of 2.27 and 1.41% between 156 and 80 K. The *c* parameter decreases by 1.02% over this range, giving an overall volume contraction of 4.64% (V = 3824.31(14) $Å^3$ at 156 K to 3646.89(11) $Å^3$ at 80 K). Upon heating, the lattice dimensions closely follow those obtained on cooling.

(b) The structural changes associated with desorption of the acetone guest molecules from **SCOF-4(Ac)** were initially investigated by heating from 260 to 350 K (Figure 4). The variable temperature diffraction data revealed a remarkable three-step process that proceeded through a partially desorbed orthorhombic phase (**SCOF-4(∼Ac)**) and a metastable desorbed tetragonal phase (***m*-SCOF-4**), to a collapsed form of the desorbed material (***c*-SCOF-4**). The **SCOF-4(Ac)** to **SCOF-4(∼Ac)** transition (290 K) is an abrupt tetragonal-to-orthorhombic ($P2_12_12$) transition, as also observed for the SCO region; however, here the splitting of peaks is much more pronounced. Conversely, the subsequent **SCOF-4(∼Ac)** to ***m*-SCOF-4** transition proceeds gradually, *via* a two phase region, as the unique *a* and *b* parameters of the orthorhombic phase progressively converge toward a single tetragonal parameter at *ca.* 310 K. From the inspection of the Bragg reflections, there is a clear decrease in the number of observed reflections for ***m*-SCOF-4** compared to the $P\bar{4}2_1c$ phase of **SCOF-4(Ac)** (specifically $\langle 0kl;$

$l = 2n \rangle$ and $\langle hk0; h + k = 2n \rangle$), with Le Bail analysis indicating the high symmetry tetragonal space group $P4/ncc$. Throughout these transitions, the overall lattice volume shows only a small decrease, from 3897.66(9) $Å^3$ at 290 K (**SCOF-4(Ac)**) to 3883.98(11) $Å^3$ at 315 K (***m*-SCOF-4**). With further heating, the lattice volume contracts to a minimum of 3870.06(17) $Å^3$ at 335 K, as the last of the acetone is removed from the pores, before partial amorphization at temperatures above 340 K to the collapsed form of the desorbed material, ***c*-SCOF-4**. This crystalline-amorphous phase transition is irreversible upon subsequent cooling.

(c, d) Despite the partial amorphization, the broad features in the diffraction data were sufficient to allow a qualitative investigation of the temperature dependence of ***c*-SCOF-4**. No significant structural changes were evident from the variable temperature diffraction data, which show only a minor thermal contraction and expansion during the 350−80−260 K temperature cycle. S-PXRD of the ***c*-SCOF-4** sample after immersion in acetone for 4 h confirmed the resorption of acetone and the recovery of the tetragonal phase, ***r*-SCOF-4(Ac)** (Table 4).

(e) A fresh sample of **SCOF-4(Ac)** was loaded and maintained under a helium atmosphere at 260 K for 3.5 h to carefully monitor the desorption process (see the Figure 4 inset). As observed for experiment (b), the desorption to the metastable apohost, ***m*-SCOF-4**, occurs *via* an intermediate partially desorbed phase, **SCOF-4(∼Ac)**. The abrupt **SCOF-4(Ac)** to **SCOF-4(∼Ac)** transition occurred after 14 min, as evidenced by a dramatic splitting of $\langle hkl; h \neq k \rangle$ reflections as the lattice transforms from tetragonal ($P\bar{4}2_1c$: a = 15.22247(15) Å, c = 16.7296(2) Å, V = 3876.63(7) $Å^3$) to orthorhombic ($P2_12_12$: a = 14.9801(3) Å, b = 15.5185(4) Å, c = 16.7061(2) Å, V = 3883.63(14) $Å^3$). The *a* and *b* parameters continue to diverge to a maximum separation of a = 14.9349(3) Å and b = 15.5458(3) Å after 54 min, before slowly converging over a further 90 min. The continuous **SCOF-4(∼Ac)** to ***m*-SCOF-4** phase transition then occurred between 130 and 140 min *via* a two-phase region. This behavior represents a scissoring/flexing of the interpenetrated layers and distortion of the pore shape during the desorption process. The *c* parameter and lattice volume remain largely unchanged throughout the desorption process, showing only a slight discontinuity across the initial **SCOF-4(Ac)** to **SCOF-4(∼Ac)** phase transition.

(f) The temperature dependence of ***m*-SCOF-4** was investigated over the temperature range 260−80−260 K. The diffraction data show a reversible phase transition at *ca.* 190 K to a lower symmetry phase. The diffraction pattern of the low symmetry phase is significantly more complex than that of the low temperature orthorhombic phase of **SCOF-4(Ac)**. Analysis of the data suggested that the symmetry lowering involves a large monoclinic superlattice structure with doubling and/or tripling of at least one of the lattice dimensions. The present data are of insufficient resolution to accurately index this phase. Qualitative peak evolution analysis of the variable temperature diffraction data showed no evidence of large changes in the lattice parameter associated with SCO behavior.

(g) The ***m*-SCOF-4** sample was maintained in the flow-cell apparatus with exposure to acetone vapor at 260 K. The *in situ* diffraction data showed the resorption process to occur within 6 min of exposure to acetone vapor, following the reverse phase transition progression of desorption: $P4/ncc$ (***m*-SCOF-4**)-to-$P2_12_12$ (***r*-SCOF-4(∼Ac)**)-to-$P\bar{4}2_1c$ (***r*-SCOF-4(Ac)**). The refined lattice parameters for ***r*-SCOF-4(Ac)** here agree closely with those observed for experiment (d) following *ex situ*

resorption from the collapsed phase, *c*-**SCOF-4** (see Table 4). In both *r*-**SCOF-4(Ac)** phases, the overall lattice volumes are marginally higher than that observed for the as-synthesized material at the same temperature, suggesting an enhanced uptake of acetone for the resorbed phases and/or a slightly different alignment of guests within the channels.

(h) Variable temperature diffraction data for *r*-**SCOF-4(Ac)** were collected with cooling from 260 to 80 K, showing notably different behavior from that observed for the as-synthesized material, **SCOF-4(Ac)**. The tetragonal-to-orthorhombic phase transition occurs at 203 K, approximately 40 K higher than that observed for **SCOF-4(Ac)**. Changes in the lattice parameters consistent with SCO behavior are evident below 122 K, with the lattice volume contracting by 3.14% between 122 and 80 K. This contraction not only occurs *ca.* 30 K lower but is also significantly smaller than the 4.64% contraction observed for **SCOF-4(Ac),** suggesting a diminished extent of spin conversion for the resorbed material. The changes in the *a* and *b* parameters for *r*-**SCOF-4(Ac)** show similar extents of contraction over the SCO region, in contrast to the markedly different extents of contractions between the two parameters for **SCOF-4(Ac)**.

(i) A fresh sample of **SCOF-4(Ac)** was loaded at 260 K under a helium atmosphere while diffraction data were collected to monitor the desorption process. Following the abrupt **SCOF-4(Ac)** to **SCOF-4(~Ac)** transition, the sample was immediately cooled and subsequently heated in the range 260–80–260 K. The temperature dependent diffraction data revealed a complex low symmetry phase below 200 K. The resolution of the present data was again insufficient for accurate indexing, but qualitative analysis suggested that this phase is closely related to the low temperature phase observed for *m*-**SCOF-4**. The peak evolution of the variable temperature diffraction data showed no evidence for SCO behavior.

Temperature-Dependent Lattice Parameters from SC-XRD. The temperature dependence of the lattice dimensions of a single-crystal sample of **SCOF-4(Ac)** was followed over the range 25–200 K (Supporting Information). The lattice dimensions were constrained to be tetragonal over all temperatures due to the pseudomerohedral twinning of the crystals (orthorhombic emulating tetragonal with equal twin components), which causes an averaging of the measured *a* and *b* parameters. Despite this limitation, the general changes in these unit cell dimensions are consistent with the **S-PXRD** data for the overlapping temperature regions (80–250 K). Most notably here, a clear difference is evident in the behavior of the quench-cooled and slow-cooled crystals, indicating a history-dependence of the spin state. For the slow-cooled crystal, the *a* parameter decreased from 15.039(8) Å at 150 K to 14.755(15) Å at 50 K, a decrease of 1.89(11)%, and the *c* parameter decreased concomitantly from 16.880(5) to 16.730(13) Å, a decrease of 0.8(8)%. Overall, the volume contracted by 4.6(2)%, from 3819(5) Å^3 at 150 K to 3642(6) Å^3 at 50 K. The initial lattice parameters at 25 K for the quench-cooled crystal were significantly larger than that observed on slow cooling (*ca.* 1.5% by volume). Upon heating, the lattice parameters first decreased sharply from 40 K to a minimum between 60 and 75 K (*ca.* 2% decrease in volume). Beyond 75 K, the lattice parameters increased sharply, converging with the results obtained upon slow-cooling at *ca.* 100 K. This behavior was evident in magnetic susceptibility measurements and is consistent with thermally induced trapping of a partially HS phase upon quench cooling (TIESST).

Thermogravimetry. When exposed to the atmosphere under ambient conditions, single crystals of **SCOF-4(Ac)** rapidly showed signs of loss of integrity, such as loss of translucence and severe cracking. Thermogravimetric analysis showed significant mass loss from 25 °C and complete desorption of the acetone guests with heating to 70 °C, beyond which the empty framework material, **SCOF-4**, appears to be stable to 150 °C. The observed mass loss of *ca.* 18% associated with the desorption of the guest species is less than the calculated value of 24.4%, indicating a significant amount of guest loss during sample preparation. Porosity was investigated by the immersion of a desorbed sample of **SCOF-4** in liquid acetone, with subsequent thermogravimetric analysis confirming the resorption of acetone into the framework.

Discussion

SCOF-4(Ac) represents a targeted variation within a series of SCOF materials that consist of doubly interpenetrating rhombic grids (2 × (4,4) nets) with the general formula $Fe(NCS)_2(L)_2 \cdot x(guest)$ (Figure 1). These materials have shown a range of remarkable guest-dependent structural and SCO features, with **SCOF-4(Ac)** providing a distinct contrast to both the host–guest and SCO properties of the earlier materials. The first of these, **SCOF-1(Et)** (Et = ethanol), exhibits a "half"-SCO where one of two crystallographically distinct iron(II) centers undergoes a spin transition; the desorption of **SCOF-1(Et)** to **SCOF-1** results in reversible pore collapse and deactivation of the SCO.[11] In contrast, the two closely related SCOFs with the more functionalized bridging ligands bpbd (**SCOF-2(Ac)**)[9] and bped (**SCOF-3(Et)**)[8] offer more robust structural motifs due to stabilizing host–host hydrogen-bonding interactions between the interpenetrated grids. Consequently, the spin transitions are retained for both the desorbed host frameworks. In contrast, the complex structure–function relationship for **SCOF-4(Ac)** is not dictated by host–host and/or host–guest hydrogen-bonding interactions. The incorporation of the less functionalized, and hence more flexible, bpe ligand in **SCOF-4(Ac)** has not only generated a SCOF with a larger solvent accessible pore volume of *ca.* 39% but has also imparted a notable flexibility within the host material. This flexibility is manifest in a remarkable series of both subtle and dramatic structural phase transitions associated with the SCO and host–guest properties of **SCOF-4(Ac)**.

The two-step nature of the spin transition in **SCOF-4(Ac)** is not only unique within SCOF materials but also represents a rare case of such behavior for SCO systems in general. Most of the reported examples of two-step (or multistep) transitions involve discrete mono- or dinuclear complexes, while only a small number of such polynuclear systems have been reported.[28,29]

(27) Létard, J.-F.; Guionneau, P.; Rabardel, L.; Howard, J. A. K.; Goeta, A. E.; Chasseau, D.; Kahn, O. *Inorg. Chem.* **1998**, *37*, 4432–4441.

(28) (a) Bartel, M.; Absmeier, A.; Jameson, G. N. L.; Werner, F.; Kato, K.; Takata, M.; Boca, R.; Hasegawa, M.; Mereiter, K.; Caneschi, A.; Linert, W. *Inorg. Chem.* **2007**, *46*, 4220–4229. (b) Niel, V.; Thompson, A. L.; Goeta, A. E.; Enachescu, C.; Hauser, A.; Galet, A.; Muñoz, M. C.; Real, J. A. *Chem.—Eur. J.* **2005**, *11*, 2047–2060. (c) Grunert, C. M.; Schweifer, J.; Weinberger, P.; Linert, W.; Mereiter, K.; Hilscher, G.; Muller, M.; Wiesinger, G.; van Koningsbruggen, P. J. *Inorg. Chem.* **2004**, *43*, 155–165.

(29) (a) Muñoz, M. C.; Gaspar, A. B.; Galet, A.; Real, J. A. *Inorg. Chem.* **2007**, *46*, 8182–8192. (b) Yamada, M.; Ooidemizu, M.; Ikuta, Y.; Osa, S.; Matsumoto, N.; Iijima, S.; Kojima, M.; Dahan, F.; Tuchagues, J. P. *Inorg. Chem.* **2003**, *42*, 8406–8416. (c) Garcia, Y.; Kahn, O.; Rabardel, L.; Chansou, B.; Salmon, L.; Tuchagues, J. P. *Inorg. Chem.* **1999**, *38*, 4663–4670.

From a structural perspective, all of these examples fall within three distinct categories. For the majority, the two-step nature results from the coexistence of two "ordered" SCO centers at all temperatures, where the subtle differences in coordination environments result in separated transitions.[29−31] Second, several cases have been reported with entirely "disordered" HS:LS intermediate states where a single crystallographic SCO site shows averaged metal−ligand bond lengths at the IP.[28,32] Finally, the rarest examples involve systems that undergo a structural phase transition associated with the SCO, where a single crystallographic site converts to two unique sites, or vice versa, upon cooling through one or both of the transitions.[33−35] In classifying the behavior of **SCOF-4(Ac)**, we consider each of its transition steps separately. For the high temperature SCO step, the rather abrupt tetragonal-to-orthorhombic structural transition, which occurs *ca.* 20 K above the onset of the first SCO step, appears to be driven sterically rather than by the SCO; that is, two inequivalent iron(II) sites exist before the onset of the half-step SCO.[36] This conclusion is perhaps best exemplified by the fact that the resorbed phase ***r*-SCOF-4(Ac)** displays the same structural transition *ca.* 90 K above a now suppressed first SCO step and that similar symmetry-lowering transitions occur in the absence of SCO in the partially- and fully-desorbed phases. As might be expected given that only very subtle changes in iron(II) geometry are expected, there is no discernible change in HS magnetic moment through this transition. In contrast to the first step, the transition back to tetragonal symmetry, and a single crystallographically distinct iron(II) site, with cooling through the low temperature step appears to be directly associated with and, at least to some extent, driven by the SCO transition. While the variable temperature SC-XRD unit cell data are not conclusive on this point due to pseudomerohedral crystal twinning, this conclusion is supported by our observation of conventional LIESST relaxation kinetics below the step, which are consistent with the absence of structural transitions. As such, **SCOF-4(Ac)** represents, to our knowledge, the first case of a multidimensional coordination framework where SCO accompanies a structural phase transition.

Systems in which two-step spin conversions drive symmetry change offer a novel means for examining the relative importance of cooperative versus anticooperative interactions between switching metal centers. For an isolated two-dimensional grid, any cooperative interactions would be expected to favor a wholly HS or LS arrangement of SCO sites, whereas anticooperative interactions would be expected to favor a checkerboard arrangement of HS and LS sites. However, recent studies of SCOF systems have established that there is little or no intraframework communication between SCO sites that are coordinatively linked through relatively long and flexible ligands similar to bpe.[8] For **SCOF-4(Ac)**, where there are no significant host−guest or host−host hydrogen-bonding interactions, the mechanism of communication therefore necessarily involves a balance between relatively subtle interactions. Structural analyses before and after the tetragonal (**SCOF-4(Ac)25**) to orthorhombic (**SCOF-4(Ac)100,150**) transition suggest that stabilization of the HS:LS state emerges principally from the rearrangement of anticooperative 4-fold edge-to-face pyridyl embraces along the crystallographic *c*-axis and cooperative thiocyanate−pyridyl interactions in the *ab*-plane, each occurring between adjacent interpenetrated nets, rather than through ligand-mediated effects within the rhombic grids. Together, these interframework interactions lead to three-dimensional rather than lower-dimensional crystal ordering of HS and LS sites,[33] albeit with a degree of pseudomerohedral twinning. The same mechanism, in reverse, may be applied to the tetragonal-to-orthorhombic transition observed at *ca.* 160 K, with the energetics of SCO not contributing to the crystal transformation energetics in this case. Interestingly, in the absence of guest species (***m*-SCOF-4**), a similar, but much more severe, symmetry-lowering transition occurs at *ca.* 200 K. This suggests that while the guests do not directly interact with the host framework, they provide a crucial structural supporting role that buffers the more severe phase transition. Further, this confirms that solvent order/disorder is not responsible for the transition. More broadly, the absence of similar symmetry-lowering transitions in the related framework phases **SCOF-2** and **SCOF-3**, which contain similar interactions, likely indicates the dominance of short interframework hydrogen bonds on the structural energetics of those systems.

The thermal trapping of substantial HS fractions (*ca.* 25%) with rapid quenching of **SCOF-4(Ac)** from ambient temperature to 25 K, as evidenced by both the magnetic and SC-XRD measurements, raises interesting questions as to the structural mechanism for this. Careful analysis of **SCOF-4(Ac)25T** indicates that it adopts the symmetry of the intermediate HS:LS phase rather than that of the ambient temperature and 25 K slow-cooled structures. The thermal trapping of this phase suggests that an activation barrier exists between this orthorhombic HS:LS structure and the tetragonal LS structure at low temperature, a point that is consistent with the observation of slow kinetics for the low temperature SCO step.[37] This trapping may occur either as a random distribution of HS:LS sites at the Fe1 site throughout an orthorhombic crystal or in crystal domains of different spin state distribution and/or symmetry, as might arise due to the different cooling rates throughout the crystal. The quenching of a high concentration of twin planes in this orthorhombic phase to emulate the tetragonal structure may also influence the extent of HS trapping, with the regions

(30) Amoore, J. J. M.; Kepert, C. J.; Cashion, J. D.; Moubaraki, B.; Neville, S. M.; Murray, K. S. *Chem.—Eur. J.* **2006**, *12*, 8220–8227.

(31) (a) Nihei, M.; Ui, M.; Yokota, M.; Han, L. Q.; Maeda, A.; Kishida, H.; Okamoto, H.; Oshio, H. *Angew. Chem., Int. Ed.* **2005**, *44*, 6484–6487. (b) Matouzenko, G. S.; Létard, J.-F.; Lecocq, S.; Bousseksou, A.; Capes, L.; Salmon, L.; Perrin, M.; Kahn, O.; Collet, A. *Eur. J. Inorg. Chem.* **2001**, 2935–2945.

(32) (a) Leita, B. A.; Neville, S. M.; Halder, G. J.; Moubaraki, B.; Kepert, C. J.; Létard, J.-F.; Murray, K. S. *Inorg. Chem.* **2007**, *46*, 8784–8795. (b) Gaspar, A. B.; Ksenofontov, V.; Reiman, S.; Gütlich, P.; Thompson, A. L.; Goeta, A. E.; Muñoz, M. C.; Real, J. A. *Chem.—Eur. J.* **2006**, *12*, 9289–9298.

(33) Neville, S. M.; Leita, B. A.; Halder, G. J.; Kepert, C. J.; Moubaraki, B.; Létard, J. F.; Murray, K. S. *Chem.—Eur. J.* **2008**,

(34) (a) Zhang, W.; Zhao, F.; Liu, T.; Yuan, M.; Wang, Z. M.; Gao, S. *Inorg. Chem.* **2007**, *46*, 2541–2555. (b) Yamada, M.; Hagiwara, H.; Torigoe, H.; Matsumoto, N.; Kojima, M.; Dahan, F.; Tuchagues, J. P.; Re, N.; Iijima, S. *Chem.—Eur. J.* **2006**, *12*, 4536–4549. (c) Boinnard, D.; Bousseksou, A.; Dworkin, A.; Savariault, J.-M.; Varret, F.; Tuchagues, J.-P. *Inorg. Chem.* **1994**, *33*, 271–281.

(35) (a) Chernyshov, D.; Hostettler, M.; Törnroos, K. W.; Bürgi, H.-B. *Angew. Chem., Int. Ed.* **2003**, *42*, 3825–3830. (b) Törnroos, K. W.; Hostettler, M.; Chernyshov, D.; Vangdal, B.; Bürgi, H. B. *Chem.—Eur. J.* **2006**, *12*, 6207–6215.

(36) We note that while it is not uncommon for electronically-driven structural transitions to precede the magnetic/electronic evidence for these in delocalized electronic systems (see: Pouget, J. P.; Regnault, L. P.; Ain, M.; Hennion, B.; Renard, J. P.; Veillet, P.; Dhalenne, G.; Revcolevschi, A. *Phys. Rev. Lett.* **1994**, *72*, 4037–4040.), no such behavior is expected in SCO systems.

(37) While slow thermal ramping through the low temperature step revealed no hysteresis, more rapid scans led to an approximately 10 K hysteresis; see the Supporting Information.

neighboring these planes expected to have nonbulk structural geometries more closely resembling the tetragonal phase.

Several interesting features emerge from the photomagnetic characterizations of **SCOF-4(Ac)**. First, the observation of a pronounced LIESST effect in a porous framework material raises the possibility of stimulating host−guest processes by light irradiation; for example, while the HS excitation observed here can be trapped only at low temperatures, bleaching of porous SCOFs to their alternate spin state at higher temperatures is expected to influence the energetics of guest desorption/sorption, particularly in small-pore systems that undergo staging mechanisms and/or activated transport. Notably, the light-induced trapped HS state in **SCOF-4(Ac)** exceeds that seen in the only other porous material yet reported to be LIESST-active, **SCOF-3(Et)**.[8] The fact that the LIESST moment exceeds that of the 50:50 HS:LS plateau suggests that the light-activated phase retains the high symmetry tetragonal structure with a random distribution of HS and LS iron(II) sites. This conclusion is supported by the observation of conventional pseudo-first-order relaxation kinetics of the trapped HS-state, since there is no indication of multistep processes, as might be expected for the relaxation from or transformation to inequivalent iron(II) sites and by the subtle difference in T(LIESST) and T(TIESST) temperatures (Figure 2 inset).

More conventionally, interest in the LIESST phenomenon is toward achieving T(LIESST) values near ambient temperatures, such that switching between LS and metastable HS states may be achieved at workable conditions.[2] While T(LIESST) values are not likely to attain high temperatures in SCOFs, LIESST measurements have been shown to be useful for qualifying the communication effect of coordinatively linking SCO centers using long bridging ligands.[8] Through comparing $T_{1/2}$ and T(LIESST) using the relationship T(LIESST) $= T_0 - 0.3T_{1/2}$, the T_0 value, which represents an empirical measure of the degree of cooperation, can be obtained[16] and used to categorize SCO systems into different families: unidentate materials show T_0 values with an upper limit of 100 K,[38] bidentate materials $T_0 = 120$ K,[38] meridional materials $T_0 = 150$ K,[39] and network materials $T_0 = 200$ K.[40] With $T_{1/2}$ values of 80 and 133 K, and hence T_0 values of 76 and 92 K, respectively, we can place **SCOF-4(Ac)** in the $T_0 = 100$ K family of compounds containing unidentate ligands. From this we conclude that, even though the SCO centers in **SCOF-4(Ac)** are linked into a network through coordination bonds, the spin state information is only weakly propagated between adjacent metal centers through the relatively flexible bpe bridging ligand and weak intermolecular contacts; similar conclusions have been drawn for related SCOFs with flexible linkers.[8]

As is the case for the related SCOF phases, and in contrast to one- and two-dimensional iron(II) coordination frameworks that incorporate the bpe ligand,[41] the doubly interpenetrated framework topology of **SCOF-4** confers nanoporosity to this framework, with the structure being retained during reversible desorption/sorption. In combination with its SCO functionality,

the flexible porosity of this material confers a highly complex structural chemistry, with the material observed to undergo a broad array of structural transformations as a function of degree of sorption and iron(II) spin state, and, in turn, to sample treatment, temperature of measurement, and thermal history (including quench/nonquench cooling). Given that no significant hydrogen-bonding interactions exist between the framework and included acetone guests, the observed transition from tetragonal-to-orthorhombic-to-tetragonal symmetry upon acetone desorption, and subsequent further transformations of the resulting metastable phase with cooling or further heating, demonstrate that the energetics of framework distortion are extremely low; this is consistent both with there being considerable flexibility within the interpenetrating rhombic grids, as conferred by the rotational freedom of the Fe-bpe-Fe linkages, and only weak interactions between these grids, allowing their scissoring and relative displacement.

The subtle framework transformations of the types described above have critical influence on the SCO properties, with the partially and fully desorbed phases being SCO inactive. Such differences appear most likely due to bulk structural effects rather than to local changes in the iron(II) second coordination sphere, as evidenced by the complete loss of SCO in the partially solvated phase **SCOF-4(~Ac)**. Similarly, the diminished SCO following acetone resorption likely reflects bulk structural change rather than local effects, with the S-PXRD data demonstrating that the *r*-**SCOF-4(Ac)** phase is structurally homogeneous and displays an abrupt tetragonal-to-orthorhombic transition and partial SCO at temperatures different from that of the parent material. The diminished SCO for this phase is likely the result of a differing degree of acetone loading and/or an alternative alignment of the acetone guest molecules within the channels to give a modified long-range framework geometry. This behavior contrasts markedly with that seen in **SCOF-1(Me)** (Me = methanol), which displays a progressive loss of SCO but no change in transition temperature with guest desorption, most likely reflecting sample heterogeneity through the desorption transition.[12]

Conclusion

Central to the development of functional porous materials, such as SCOFs and other advanced MOFs, are investigations of the relative importance of the diverse range of host−host, host−guest, and guest−guest interactions with respect to their often highly complex structure−function relationships. The results presented here demonstrate that considerable care is required to accurately elucidate the nature of both SCO transitions and intricate host−guest processes[13,15,42] in this class of materials. This will be of particular importance in future studies of the magnetostructural effects of systematic guest variation within porous SCOFs.

SCOF-4(Ac) represents a unique example of a multidimensional two-step SCO system where a crystallographic phase transition describes a three-dimensional ordering of a HS:LS intermediate. Somewhat unconventionally, this structural perturbation appears to be stabilized principally through a three-dimensional network of weak interframework interactions rather than through direct bonding linkages. The extreme subtlety of the transition highlights the case that, with the possible exception of isolated discrete polynuclear systems and materials that contain pronounced random disorder when in their single spin-state, at least short-range and/or low dimensional ordering of HS and LS sites are likely to exist in all stable mixed-spin-

(38) Létard, J.-F.; Capes, L.; Chastanet, G.; Moliner, N.; Létard, S.; Real, J.-A.; Kahn, O. *Chem. Phys. Lett.* **1999**, *313*, 115−120.
(39) (a) Carbonera, C.; Costa, J. S.; Money, V. A.; Elhaik, J.; Howard, J. A. K.; Halcrow, M. A.; Létard, J. F. *Dalton Trans.* **2006**, 3058−3066. (b) Money, V. A.; Costa, J. S.; Marcén, S.; Chastanet, G.; Elhaik, J.; Halcrow, M. A.; Howard, J. A. K.; Létard, J. F. *Chem. Phys. Lett.* **2004**, *391*, 273−277. (c) Marcén, S.; Lecren, L.; Capes, L.; Goodwin, H. A.; Létard, J. F. *Chem. Phys. Lett.* **2002**, *358*, 87−95.
(40) Shimamoto, N.; Ohkoshi, S.; Sato, O.; Hashimoto, K. *Inorg. Chem.* **2002**, *41*, 678−684.

state SCO systems[30,33,35,43] and that members of the "order-to-disorder" category of two-step SCO systems have likely been misassigned.

In contrast to other reported SCOFs, the SCO properties of the highly flexible **SCOF-4** host lattice are very strongly influenced by minor structural perturbations induced by guest sorption/desorption and temperature. In addition to providing new insight into the SCO phenomenon, the use of SCO as a sensitive probe for structural change points to the possible application of flexible porous SCOFs in molecular sensing, with activation/deactivation or modification of SCO properties in a guest-dependent fashion leading to readily observable macroscopic changes, e.g., in color. Conversely, SCO induced by

variation in temperature and light-irradiation (here, the largest effect yet seen in a porous SCOF) provides a novel mechanism for the modification of framework structure and resulting pore chemistry. Such a property points, ultimately, to the possible generation of advanced multifunctional materials that allow some degree of external control over host−guest processes.

Supporting Information Available: Additional magnetic susceptibility data, thermogravimetric data, crystallographic information files and special refinement details, ORTEP diagrams, and complete figures of S-PXRD data analysis (peak evolutions, representative patterns and fits, refined lattice parameters). This material is available free of charge via the Internet at http://pubs.acs.org.

JA8068038

(41) (a) Wang, C. C.; Dai, S. C.; Lin, H. W.; Lee, G. H.; Sheu, H. S.; Lin, Y. H.; Tsai, H. L. *Inorg. Chim. Acta* **2007**, *360*, 4058–4067. (b) Matouzenko, G. S.; Perrin, M.; Le Guennic, B.; Genre, C.; Molnar, G.; Bousseksou, A.; Borshch, S. A. *Dalton Trans.* **2007**, 934–942. (c) Garcia-Couceiro, U.; Castillo, O.; Luque, A.; Garcia-Teran, J. P.; Beobide, G.; Roman, P. *Cryst. Growth Des.* **2006**, *6*, 1839–1847. (d) Morita, T.; Asada, Y.; Okuda, T.; Nakashima, S. *Bull. Chem. Soc. Jpn.* **2006**, *79*, 738–744. (e) Morita, T.; Nakashima, S.; Yamada, K.; Inoue, K. *Chem. Lett.* **2006**, *35*, 1042–1043. (f) Konar, S.; Zangrando, E.; Drew, M. G. B.; Mallah, T.; Ribas, J.; Chaudhuri, N. R. *Inorg. Chem.* **2003**, *42*, 5966–5973. (g) Hernandez, M. L.; Barandika, M. G.; Urtiaga, M. K.; Cortes, R.; Lezama, L.; Arriortua, M. I.; Rojo, T. *J. Chem. Soc., Dalton Trans.* **1999**, 1401–1406.

(42) Maji, T. K.; Uemura, K.; Chang, H. C.; Matsuda, R.; Kitagawa, S. *Angew. Chem., Int. Ed.* **2004**, *43*, 3269–3272.

(43) Klingele, M. H.; Moubaraki, B.; Cashion, J. D.; Murray, K. S.; Brooker, S. *Chem. Commun.* **2005**, 987–989.